

**Free-electron production from nucleotides upon collision with charged carbon ions**

Adrian Bøgh Salo and Andreas Alberg-Fløjborg

*Department of Physics, Chemistry, and Pharmacy, University of Southern Denmark, Campusvej 55, DK-5230 Odense M, Denmark*

Iliia A. Solov'yov\*

*Department of Physics, Chemistry, and Pharmacy, University of Southern Denmark, Campusvej 55, DK-5230 Odense M, Denmark  
and On leave from A. F. Ioffe Physical-Technical Institute, Politechnicheskaya 26, 194021 St. Petersburg, Russia*

(Received 2 February 2018; revised manuscript received 9 June 2018; published 5 July 2018)

Ion-beam cancer therapy has become increasingly favored worldwide in treatment of certain types of cancer over the last decade. Whereas the clinical effects of the therapy are well documented, the understanding of the underlying physical mechanisms is somewhat incomplete. The problem arises due to the multiscale nature of the effects involved in ion-beam cancer therapy, as the effects range from quantum-mechanical to macroscopic scales. The present study investigates the production of free electrons in the vicinity of the Bragg peak through quantum-mechanical simulations of the collision between a  $C^{4+}$  ion with a cytosine-guanine nucleotide pair taken from a DNA double helix. Time-dependent density-functional theory was employed using the OCTOPUS 6.0 software. The results show that such a collision triggers the release of a large amount of electrons into the cellular environment, as only a fraction is captured by the  $C^{4+}$  ion. Furthermore, it is demonstrated that the impact angle and projectile kinetic energy have much more influence on the number of ejected electrons than the impact parameter.

DOI: [10.1103/PhysRevA.98.012702](https://doi.org/10.1103/PhysRevA.98.012702)**I. INTRODUCTION**

In recent years interest in the radiation damage produced by charged ions has intensified due to the discovery of its lethal effects on certain types of cancer, such as, e.g., brain tumors [1,2]. These effects have culminated in the development of a unique cancer treatment technique called the ion-beam cancer therapy (IBCT) [1,2].

One of the key elements that makes IBCT significantly different from photon therapy is the nonuniform distribution of the radiation dose along the projectile path [1]. Almost all of the dose in IBCT is delivered at the so-called Bragg peak, which is located at a certain depth inside the biological medium, and depends on the projectile ions [3–6].

Another key difference of the IBCT from photon therapy is the formation of secondary particles such as electrons and free radicals [3,7–9], which are produced around the Bragg peak in larger numbers and with higher densities than those produced in photon therapy. The angular distribution of the secondary particles is largely uniform [8], and it is mostly these particles that are the cause of various intracellular damage, rather than the charged projectile ion itself [8,9]. It is thus of great importance to understand the mechanics of free radicals and secondary electron production upon collision of a charged ion with the biological target, and furthermore, to describe how their dynamics could lead to biological damage, which in the end might cause cell apoptosis and death [8,9].

To understand the effects underlying IBCT on a tumor, or any other biological system, it is necessary to look at

the physics of radiation interaction with biological systems through the multiscale approach [8–11], which allows us to build a bridge from the microscopic effects on the level of electrons, to the cellular macroscopic scale.

The present study examines the production of free electrons in the vicinity of the Bragg peak by employing quantum-mechanical simulations of the collision between a charged carbon ion, specifically,  $C^{4+}$ , and a pair of nucleotides from a deoxyribonucleic acid (DNA) double strand, specifically, cytosine and guanine as depicted in Fig. 1. The cytosine-guanine pair is a common base pair in the DNA double helix and it is studied here in order to connect the effects of a  $C^{4+}$  ion collision with the possible damage produced in a DNA molecule. A deeper understanding of the dynamics in such a collision might pave the way for constructing more accurate multiscale models, potentially opening the possibility for making more accurate dose calculations.

**II. METHODS****A. Time-dependent density-functional theory**

The current study employs density-functional theory (DFT) [12,13] to study the quantum-mechanical dynamics of the multiatomic cytosine-guanine system. In DFT the electronic wave functions are uniquely determined by the electronic density, i.e.,  $\psi_i(\mathbf{r}) = \psi_i(\rho_e(\mathbf{r}))$ , where  $\mathbf{r}$  indicates the position in three-dimensional (3D) space and  $\rho_e(\mathbf{r}) = \sum_{i=1}^n |\psi_i(\mathbf{r})|^2$  denotes the electronic density [13–15]. Here  $n$  represents the number of occupied electronic states in the linear combination of atomic orbitals which make up the electronic wave functions and satisfies the condition  $\int_{-\infty}^{\infty} |\psi_i(\mathbf{r})|^2 d\mathbf{r} = 1$ . The electronic densities are obtained from the Kohn-Sham (KS) equations

\*ilia@sdu.dk

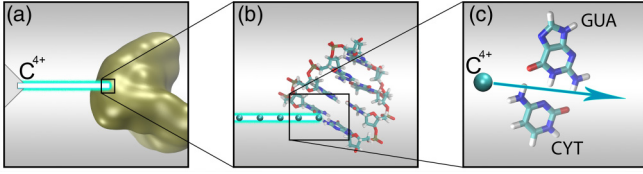


FIG. 1. A beam of carbon ions hits a piece of DNA in a cancer tumor (a). In this study the focus is on examining how electron release, electron capture, and energy deposition is affected by the collision between a highly charged carbon ion from the beam and a piece of a DNA strand (b). Here, a cytosine (CYT)-guanine (GUA) pair is chosen as a representative target (c).

[12,13] relating the energy  $\epsilon_i$  of the  $i$ th state to the electronic wave function  $\psi_i(\mathbf{r})$  via the self-consistent field (SCF) [13] approximation:

$$\left[ -\frac{1}{2}\nabla^2 - \sum_{I=1}^N \frac{Z_I}{|r-r_I|} + \frac{1}{2} \int \frac{\rho_e(\mathbf{r}')}{|\mathbf{r}-\mathbf{r}'|} d\mathbf{r}' + V_{XC}(\rho_e(\mathbf{r})) \right] \psi_i(\mathbf{r}) = \epsilon_i \psi_i(\mathbf{r}). \quad (1)$$

Here the Hartree, i.e., natural system of units, was used, with  $\hbar = m_e = |e| = 1$ ,  $Z_I$  is the atomic charge of an atom  $I$  from the present  $N$  atoms in the systems, and  $V_{XC}$  is the exchange correlation functional defined by the exchange correlation energy as  $V_{XC}(\rho_e) = \frac{\delta E_{XC}(\rho_e)}{\delta \rho_e}$ .

The time evolution of the wave function can be described by the time-dependent density-functional theory (TDDFT) [15], where electronic density is evolved in time by propagating the time-dependent Kohn-Sham (TDKS) equations:

$$\left[ -\frac{1}{2}\nabla^2 - \sum_{I=1}^N \frac{Z_I}{|r-r_I|} + \frac{1}{2} \int \frac{\rho_e(\mathbf{r}',t)}{|\mathbf{r}-\mathbf{r}'|} d\mathbf{r}' + v_{\text{ext}}(\mathbf{r},t) + V_{XC}(\rho_e(\mathbf{r},t)) \right] \psi_i(\mathbf{r},t) = i \frac{\partial}{\partial t} \psi_i(\mathbf{r},t). \quad (2)$$

Here  $v_{\text{ext}}(\mathbf{r},t)$  is any time-dependent potential externally applied to the system. The TDKS equations are solved numerically by using a time propagator, where the density of the electronic wave functions and their time derivative in their initial states are related to the next time step in the time evolution of the system.

## B. Computational setup

The cytosine-guanine (CYT+GUA) pair used here to represent the molecular target was geometrically optimized using the GAUSSIAN 09 [16] program with CAM-B3LYP [17] model chemistry and the 6-31G(d) basis set [18]. All calculations employed the program OCTOPUS 6.0 [19–21] for the TDDFT calculations in a spin-polarized setup accounting for self-interaction correction to density functionals by employing the Perdew-Zunger method [22] on an X3LYP extended hybrid DFT functional [23] on a regular mesh in real space [19]. The TDDFT calculations were carried out using approximated

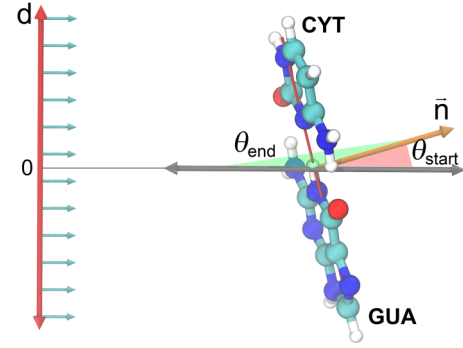


FIG. 2. System setup used in the simulations. The impact parameter  $d$  is shown together with the impact angle  $\theta$ .  $d$  is varied along the red thick vector whose projection on the plane of the CYT+GUA pair is indicated by a thin red line.  $d = 0$  corresponds to collisions close to the center of mass of the CYT+GUA pair, while the directions of the  $\text{C}^{4+}$  ion motion for other values of  $d$  are indicated by cyan arrows. The impact angle  $\theta_{\text{start}} < \theta < \theta_{\text{end}}$  is defined as the angle between the CYT+GUA pair normal vector  $\hat{n}$  and the  $\text{C}^{4+}$  ion shooting direction indicated by the gray vectors for the outermost cases characterized through  $\theta_{\text{start}}$  and  $\theta_{\text{end}}$ , where  $\theta_{\text{start}} = 18^\circ$  and  $\theta_{\text{end}} = 158^\circ$ .  $\theta = 90^\circ$  represents an in-plane collision.

enforced time-reversal symmetry (AETRS) [24] as the propagator for the TDKS equations.

Three sets of simulations were considered in order to study the effects of varying collision parameters, specifically, (1) the initial kinetic energy of the  $\text{C}^{4+}$  ion projectile,  $E_{\text{kin}}$ , (2) the impact parameter of the projectile,  $d$ , and (3) the collision angle between the  $\text{C}^{4+}$  ion impact direction and the plane of the CYT+GUA pair,  $\theta$ . The simulations were set up as follows:

(1) Varying  $E_{\text{kin}}$ : 13 simulations were set up with the initial kinetic energy  $E_{\text{kin}}$  of the  $\text{C}^{4+}$  ion varying in the interval from 0.006 MeV to 3.60 MeV, as shown in Table S1 in the Supplemental Material (SM) [25].

(2) Varying impact parameter  $d$ : 18 simulations were set up such that nine were performed for  $E_{\text{kin}} = 1.21$  MeV, and nine simulations were performed for  $E_{\text{kin}} = 3.60$  MeV. The impact parameter was varied as outlined in Table S2 of the SM while its definition is shown in Fig. 2. Both system setups with varying kinetic energy and the impact parameter have assumed a collision impact angle of  $\theta = 23^\circ$ . The impact angle is defined such that  $\theta = 90^\circ$  represents an in-plane collision where the  $\text{C}^{4+}$  ion first hits the CYT nucleotide. The angle of  $\theta = 0^\circ$  and  $\theta = 180^\circ$  represents the through-plane collision with the  $\text{C}^{4+}$  ion traveling parallel or antiparallel to the vector perpendicular to the plane of the CYT+GUA pair target, see Fig. 2.

(3) Varying impact angle  $\theta$ : 22 simulations were set up such that 11 were performed for  $E_{\text{kin}} = 1.21$  MeV, and 11 simulations were performed for  $E_{\text{kin}} = 3.60$  MeV. The impact angle  $\theta$  was varied as shown in Table S3 of the SM within an interval of  $18^\circ \leq \theta \leq 158^\circ$ , as depicted in Fig. 2.

The ground-state wave function for each simulation was calculated using the SCF [12,13] approach on a linear combination of atomic orbitals (LCAO) [13,26] constructed in a simulation box with a specified spatial discretization of  $\Delta x \times \Delta y \times \Delta z = 0.2 \text{ \AA} \times 0.2 \text{ \AA} \times 0.2 \text{ \AA}$  and reflecting boundary conditions. This precollision LCAO wave function was

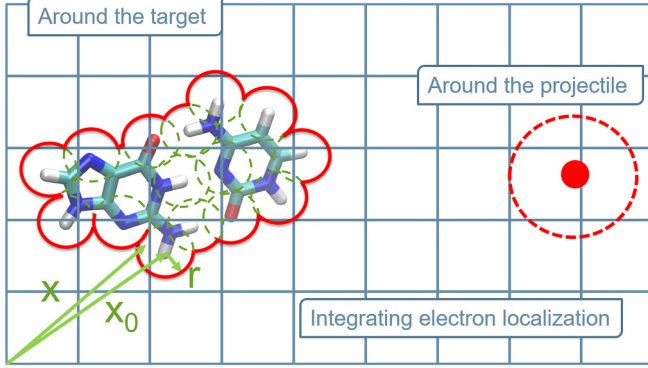


FIG. 3. Quantifying the collision process. Visual representation of how the electronic densities were integrated in the CUBECAT analysis software, see SM [25]. It is reasoned that the mismatch between the cumulative electronic densities localized around the  $C^{4+}$  ion, the CYT+GUA pair, and the total amount of electrons in the system indicates that a number of free electrons are released upon collision.

constructed from the atomic orbitals for the atoms of the target composed from standard pseudopotential species provided in OCTOPUS 6.0 [19–21]. Subsequently, the  $C^{4+}$  ion was inserted into the system close to the edge of the simulation box, after which TDDFT calculations were performed. Such an approach for constructing the wave function ensures the  $C^{4+}$  ion being devoid of valence electrons at the very beginning of the simulations. The simulation box size was chosen to be 18–20 Å along the directions perpendicular to the  $C^{4+}$  trajectory. The box dimension collinear with  $C^{4+}$  ion movement was scaled to accommodate longer simulations for higher  $E_{\text{kin}}$ , varying from 40 to 72 Å (see Tables S1–S3 [25]).

### C. Analysis methods

To analyze the electronic dynamics one should consider the evolution of the electronic densities  $\rho_e(\mathbf{r})$  around the selected parts of the system as a function of the  $C^{4+}$  passing distance relative to the target molecule. The analysis of the electronic densities was accomplished by an in-house software, CUBECAT (see SM [25]), that integrates the electronic densities within a discrete sphere around a predefined part of the system as visually conceptualized in Fig. 3. The volume integral is computed as

$$\int_0^r d^3\mathbf{r} \rho_e(\mathbf{r}) \simeq \sum_{\mathbf{x} \in X} \rho_{\mathbf{x}} \Theta(r - |\mathbf{x}_0 - \mathbf{x}|), \quad (3)$$

$$\Theta(x) = \begin{cases} 0 & \text{for } x < 0 \\ 1 & \text{for } x \geq 0 \end{cases}$$

where  $r$  is the radius of integration in Å,  $\mathbf{x}_0$  is the center around which the integration is performed,  $\mathbf{x}$  denotes the coordinate vector of the current voxel,  $X$  is the set of all voxels in the simulation grid,  $\rho_{\mathbf{x}}$  is the electronic density at voxel  $\mathbf{x}$ , and  $\Theta(x)$  is the Heaviside step function. For this study a radius  $r = 2.0$  Å has been chosen as the integration radius, and the integral is computed such that the integration radius extends from each individual atom, thereby tracing the shape of the

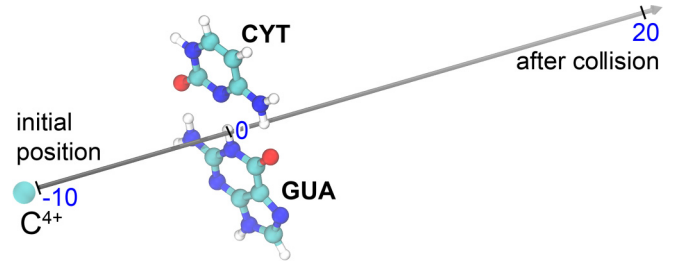


FIG. 4. Computational setup of the  $C^{4+}$  central collision. The  $C^{4+}$  ion travels through the center of mass of the CYT+GUA pair at an impact angle of  $\theta = 23^\circ$  with respect to the normal vector  $\tilde{n}$  of the molecular plane. When the  $C^{4+}$  ion travels 20 Å after passing the target, the collision event is considered completed, and this point is used as a reference for calculation and comparison of electronic density changes in the system. Note that for the initial kinetic energies of  $E_{\text{kin}} = 0.006$  MeV and  $E_{\text{kin}} = 0.036$  MeV the collision is considered complete at shorter distances after passing the CYT+GUA pair.

target molecule more accurately, reducing potential electron overcounting.

Since OCTOPUS [19–21] computes the electronic densities at the real-space grid points of the simulation box [19], the computed densities correspond to an infinitesimal volume element. The contribution of each volume element  $\mathbf{x}$ , denoted as  $c_{\mathbf{x}}$ , is then

$$\rho_{\mathbf{x}} = c_{\mathbf{x}} s^3, \quad (4)$$

where  $s = 0.2$  Å is the side length of each voxel in Å.

## III. RESULTS

The results computed in this study illustrate the dynamics of electrons from the CYT+GUA pair during and after the collision with a  $C^{4+}$  ion and provide insight on the stopping power of the same ion in a biological medium.

### A. Electron dynamics

A useful characteristic for electron density dynamics analysis is the electronic density change  $\Delta\rho_e$ , which can be computed for either the target CYT+GUA pair or the projectile ion. The electronic density change is first evaluated for the central collision, illustrated in Fig. 4 for varying initial kinetic energies of the projectile ion. In this case  $C^{4+}$  hits the center of mass of the target at an impact angle of  $\theta = 23^\circ$ ; see Fig. 2 for the impact angle definition. The initial kinetic energy of the inbound  $C^{4+}$  ion is varied from 0.006 MeV to 3.60 MeV, while the ion approaches the nucleotide pair from a distance of 10 Å. Figure 5(a) shows the change in the electronic density of the target CYT+GUA pair as a function of projectile ion traveled distance with respect to its initial kinetic energy. The change in the electronic density of the CYT+GUA pair manifests rapidly when the  $C^{4+}$  ion leaves the nucleotide pair over a time period of 200–300 as. In most cases the collision results in the removal of several electrons from the nucleotide pair. Figure 5(a) reveals that the decrease in the electronic density surrounding the nucleotide pair occurs mainly around the point where the ion has traveled around 10–11 Å. For the

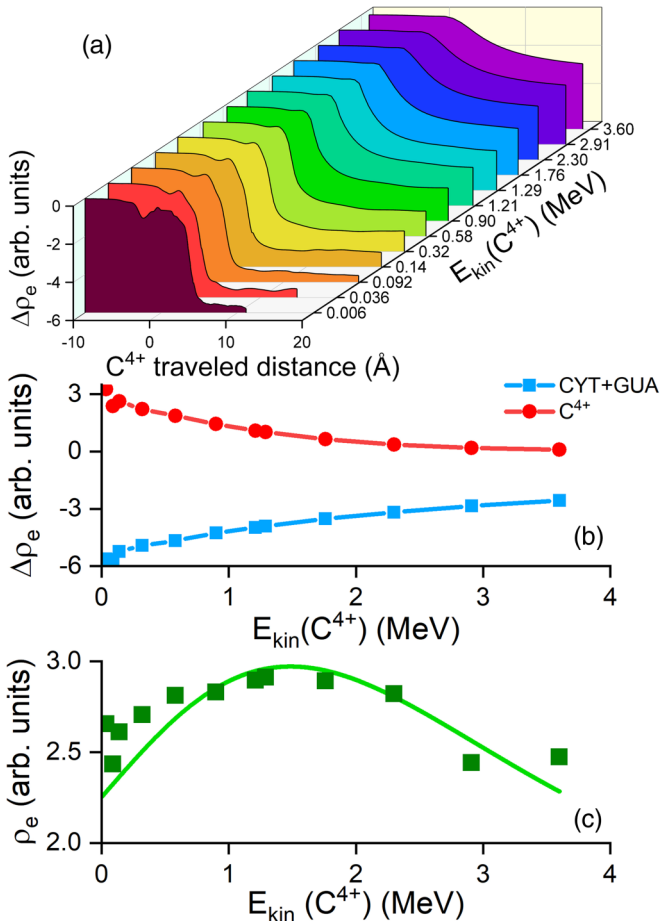


FIG. 5. Electronic density change of the CYT+GUA pair. (a) The change in electronic density  $\Delta\rho_e$  around the CYT+GUA pair during collision, see Fig. 3. Each plot corresponds to a different value of the initial kinetic energy of the  $C^{4+}$  ion, given in units of MeV. The disturbance of the electronic density starts when the  $C^{4+}$  ion approaches the target, and the electronic density surrounding the nucleotide pair starts to drop after the  $C^{4+}$  ion has left the target. The interaction is initiated earlier for lower kinetic energies of the  $C^{4+}$  ion. (b) The change of the electronic densities of the  $C^{4+}$  ion (dots) and the CYT+GUA pair (squares) after the collision is displayed as a function of initial kinetic energy of the projectile. The disturbance of the electronic density during the ion's passage through the molecule increases for smaller energies. (c) Electronic density corresponding to the free electrons released into the system during collision, i.e., the electronic density not localized around either the CYT+GUA pair or the  $C^{4+}$  ion. The curve peaks at around 1.21 MeV.

low energy of 0.006 MeV, the electronic density of the target is, however, perturbed significantly before the ion reaches the nucleotide pair. In this case the target CYT+GUA pair first loses some electronic density, which is then acquired back, as revealed by a profound dip in the plot in Fig. 5(a). This dip is also visible for higher energies; however, it becomes less pronounced as the projectile ion moves faster. The observed behavior clearly indicates that there is a fluctuating charge exchange between the projectile ion and the target molecule in the studied collision.

The distance at which the electronic density of the target drops is characteristic, as the ion is initially placed 10 Å away

from the target, see Fig. 4. Note that the perturbation of the electronic densities is similar for almost all the initial values of the  $C^{4+}$  kinetic energy, as the change in the electronic density around the nucleotide pair occurs mainly during a brief time interval after the ion's passing; this time period varies only slightly between the different initial energies of the  $C^{4+}$  projectile.

Figure 5(b) shows the release of electrons from the CYT+GUA pair and the recapture of electrons by the trespassing  $C^{4+}$  ion with respect to its initial kinetic energy. The total electronic density, corresponding to the number of electrons released into the system, is shown in Fig. 5(c). A larger effect on the number of ejected electrons in the system is observed when the  $C^{4+}$  ion collides with lower initial kinetic energy. However, not all electrons from the target remain released freely into the system but are recaptured by the  $C^{4+}$  ion, as is additionally evidenced in supporting videos S1, S2, S3, and S4 in the SM. The supporting videos depict with a green semitransparent surface the positive-valued change in the electron density as the system evolves. In other words, the cloud features locations in the system where excessive electrons delocalize, as compared to the unperturbed case. The red curve in Fig. 5(b) indicates that at lower initial energies, the  $C^{4+}$  ion captures significantly more electrons, increasing at 0.006 MeV, which is also the lowest studied energy. However, the number of electrons released into the system and thereby not located around either the CYT+GUA pair or the  $C^{4+}$  ion peaks at around 1.21 MeV, as shown in Fig. 5(c) by a fitted line. This is consistent with expectation based on the position of the Bragg peak for a  $C^{6+}$  ion being located at around 0.1 MeV/u when taking into account the decreasing charge of the projectile ion as it propagates through the biological tissue [4–6,8].

The  $C^{4+}$  ion creates a large disturbance in the electronic cloud as it travels through the CYT+GUA pair, see the supporting video S1 [25]. The change in the electronic density around the CYT+GUA pair becomes apparent shortly before the collision with the  $C^{4+}$  ion, as confirmed by Fig. 5(a).

Figures 6(a)–6(d) show the effects of varying the impact parameter  $d$  and the impact angle  $\theta$  on the change in the electronic densities of both the ion and the nucleotide pair. Variations of the impact parameter seem to have a small but noticeable influence on the release of electrons after the collision for both of the studied energies. The electron capture by the  $C^{4+}$  ion is significantly larger at 1.21 MeV than at 3.6 MeV, as is the net release of electrons into the system. The latter observation reflects that the maximal number of free electrons released from the target is expected for  $E_{kin} = 1.21$  MeV, as predicted in Fig. 5(c). The variations of the electronic density loss and free electron production by the target at around  $d = 0–1$  Å indicate a less dense distribution of the electronic density around the center of the nucleotide pair, resulting in fewer electrons being ejected. Furthermore, the nonuniform distribution of the electronic density of free electrons with varying impact parameters in Fig. 6(c) suggests variations in the topological distribution of the electronic density along the CYT+GUA pair, which can be probed in the collision process.

Varying the impact angle  $\theta$  has a significant effect on the overall release of electrons from the nucleotide pair following the collision, see Figs. 6(b) and 6(d). The number of electrons

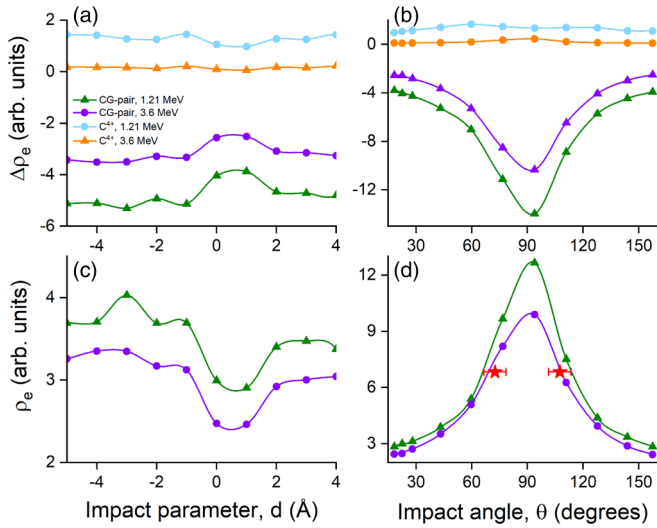


FIG. 6. Electronic density change is influenced by the impact parameters. (a) Varying the impact parameter  $d$  (see Fig. 2) has relatively little effect on the change in the electronic densities, both around the projectile ion and the target. (b) Electronic density changes around the projectile ion and the target molecule are perturbed significantly as the impact angle  $\theta$  (see Fig. 2) changes, peaking around the impact angle of  $90^\circ$ , corresponding to the longest  $C^{4+}$  ion passage distance through the CYT+GUA pair. (c) Electronic density representing the electrons released into the system and thereby not located around either the CYT+GUA pair or the  $C^{4+}$  ion for the studied impact parameter,  $d$ . (d) Electronic density of electrons released into the system peaks around an impact angle of  $\theta = 90^\circ$  mirroring the disturbance of the electronic density surrounding the CYT+GUA pair depicted in (b). Prediction for electron loss in water with a penetration depth of 1 nm for  $E_{\text{kin}} = 1.2$  MeV are illustrated by red stars, corresponding to the angle with a similar penetration depth in the nucleotide pair [7]. All density changes have been computed for two values of the initial kinetic energies  $E_{\text{kin}} = 3.6$  MeV (blue, violet) and  $E_{\text{kin}} = 1.21$  MeV (green, yellow).

released from the collision into the system varies from 2 to 12 electrons, whereas changing the impact parameter  $d$  only shifts this value by approximately one electron. The resulting release of electrons into the system shown in Fig. 6(d) increases significantly for  $\theta \rightarrow 90^\circ$ , corresponding to an in-plane collision, for which almost all missing electrons from the CYT+GUA pair become delocalized in the surrounding system. The net release of electrons after the collision seems to depend on the initial kinetic energy, and similarly for the impact parameter; see also the supporting video S4 in the SM [25].

Figure 6(d) features a comparison with previous work on electron production in water upon collision with a  $C^{4+}$  ion [7]. The passage distance of the projectile ion of about 1 nm corresponds to a value of  $\theta \simeq 73^\circ$  or  $\theta \simeq 107^\circ$  in the present simulation. The prediction of earlier studies are indicated in Fig. 6(d) by the red stars, and the comparison, reveals that for both ion trajectories at  $73^\circ/107^\circ$  the results of the earlier calculation are close to the present simulations with  $E_{\text{kin}} = 3.6$  MeV and  $E_{\text{kin}} = 1.21$  MeV.

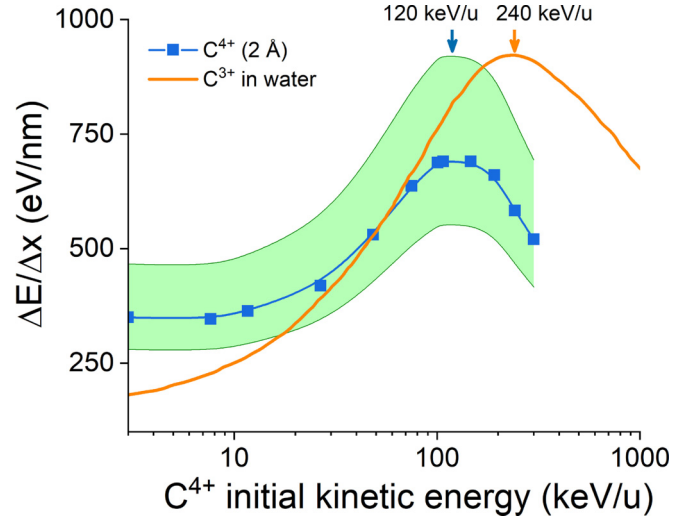


FIG. 7. Stopping power of the  $C^{4+}$  ion. Comparison of the stopping power of the  $C^{4+}$  ion in the CYT+GUA pair collisions (squares) with the stopping power of  $C^{3+}$  ion in water (orange line) [27]. The effective interaction distance of the  $C^{4+}$  ion with the CYT+GUA pair is assumed to be  $2 \pm 0.5$  Å based on the van der Waals radius, leading to a spread out distribution highlighted by a green color. The maximum stopping power for the  $C^{4+}$  ion in the CYT+GUA pair collision and for the  $C^{3+}$  ion in water is indicated by the blue and the orange arrows, respectively.

### B. Projectile stopping power

The stopping power of the projectile ion is defined as

$$S(E) = -\frac{dE}{dx}, \quad (5)$$

where  $E$  is the kinetic energy of the projectile and  $x$  is the traveled distance.

Since the simulations were done for a collision with a target in vacuum rather than through a continuous medium, the stopping power of the projectile can be approximated as

$$S \approx \frac{E_0 - E_1}{\Delta x_{\text{eff}}} = \frac{\Delta E}{\Delta x_{\text{eff}}}, \quad (6)$$

where  $E_1$  is the kinetic energy of the  $C^{4+}$  ion after traversing the CYT+GUA pair,  $E_0$  is the initial kinetic energy of the projectile ion, and  $\Delta x_{\text{eff}}$  is the effective interaction distance between the  $C^{4+}$  ion and the target molecule. The effective interaction distance between the  $C^{4+}$  ion and the CYT+GUA pair used to compute the stopping power of the  $C^{4+}$  ion is estimated to be  $\Delta x_{\text{eff}} = 2 \pm 0.5$  Å based on the van der Waals radius for atoms being 1–2 Å. Figure 7 shows that the stopping power obtained from simulations peaks at  $\sim 0.12$  MeV/u, indicated by the blue arrow, thereby differing by a factor of 2 compared to the curve measured in bulk water [27], for which the peak is around  $\sim 0.24$  MeV/u as indicated by the orange arrow. The comparison of the two curves suggests that they are shifted one with respect to another, overestimating the stopping power of lower kinetic energies as compared to a previous result [27] but otherwise reproducing the same trend. The peak at around 0.1 MeV/u matches closely the peak shown in Fig. 5(c), thereby further implicating the location of the Bragg peak to be around 0.12 MeV/u for the present

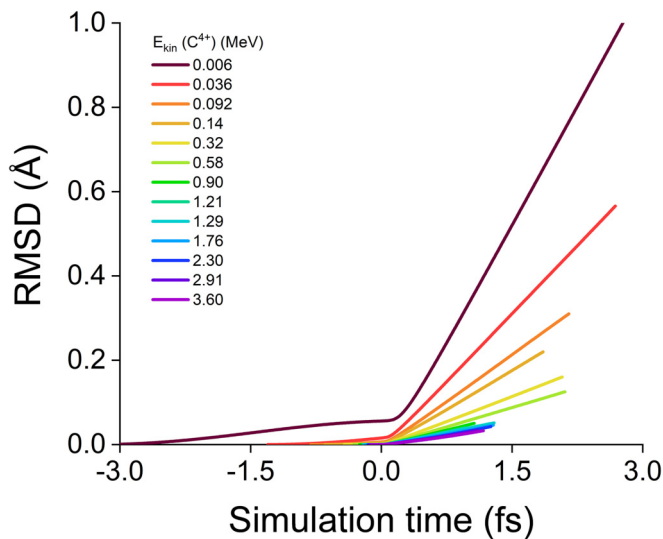


FIG. 8. The root-mean-square deviation (RMSD) of the atoms in the nucleotide pair. The RMSD values for various initial kinetic energies of the  $C^{4+}$  ion. Each line corresponds to a different value of the initial kinetic energy of the  $C^{4+}$  ion, given in units of MeV color coded in the legend. The simulation time instance of 0.0 fs corresponds to the collision, i.e., a point when the projectile ion hits the center of the target CYT+GUA pair. Linearly extrapolating the line for 0.006 MeV suggests that an RMSD of  $\sim 1$  Å is reached at around 3 fs.

study. The deviations in the present results are likely due to the fact that the nucleotide pair is not a continuous medium, as opposed to the earlier assumptions [27], where the bulk water was investigated. The difference in the total charge of the projectile is also affecting the discrepancies between earlier estimates and the present result.

### C. Spatial effects

A related aspect of the studied collision process is the question of nuclear dynamics. Analysis shows that during the course of the simulations, the geometrical arrangement of the nucleotide pair is almost static as supported by the supplementary video S5 [25]. The root-mean-square deviation (RMSD) of the atoms in the system is on the order of 0.1 Å prior collision, as shown in Fig. 8. Extrapolation of the steepest RMSD curve for 0.006 MeV in Fig. 8 delivers a RMSD value of  $\sim 1$  Å after 3 fs, which is a significantly larger timescale than that of the electronic processes, and thus atomistic movements can be safely neglected.

## IV. CONCLUSION

The performed simulations provide evidence that a  $C^{4+}$  ion disturbs the nucleotide pair system enough to allow the

formation of free electrons that have the possibility to interact with the surrounding medium in a cell, thereby creating free radicals or eventually directly damaging the DNA, causing single- or double-strand breaks. It was found that the number of free electrons which might be formed during the collision depends on a number of collision parameters. The most significant of these with regards to the removal of electrons from the nucleotide pair are the kinetic energy of the incoming ion and the incident impact angle. The total number of electrons released into the system after the collision seems to increase for lower energies and become most prominent for  $E_{\text{kin}} \approx 1.21$  MeV, which is consistent with the fact that most of the ion's energy should be deposited around the Bragg peak, where the ion's kinetic energy is significantly lower than when it entered the medium. The simulations involving rotation of the target molecule show that a significant increase of the number of ejected electrons from the CYT+GUA pair is possible; for two exemplary values of the initial energy of the  $C^{4+}$  ion the impact angle  $\theta$  shows a factor of 6 influence on the number of ejected electrons.

The CYT+GUA pair represents a nonhomogeneous biological component present in systems of interest to the studies of collisions in biological tissue with highly charged particles and it is therefore of interest to study the likely event of a charged ion collision with the nucleotide pair or a similar biological molecule. The results of this study are consistent with the multiscale model [3], where it was suggested that a highly charged carbon ion in the IBCT creates an outburst of free electrons in the vicinity of the Bragg peak of the ion. However, the present results also reveal the necessity of using more computationally demanding models to incorporate the effects of the nonhomogeneity in biological systems, which seems to highly influence the outcome in ion collisions, such as those which are occurring in the IBCT.

The present study suggests a need for further theoretical and computational analysis, such as, for example, the calculation of collision cross sections and the stopping power of the medium, in a more systematic fashion, thereby coupling the theoretical models and simulated results to observable parameters that can subsequently be investigated experimentally. The simulation data produced in this study permit further characterization of the directionality and velocity distributions of the ejected electrons and should be elaborated further to deliver an estimate of nucleotide fragmentation rates, as well as electron recombination times. These can be obtained from more systematic TDDFT calculations coupled with conventional quantum chemistry and classical molecular dynamics.

## ACKNOWLEDGMENTS

The authors would like to thank the Lundbeck Foundation, Danish Councils for Independent Research, and the Russian Science Foundation (Grant No. 17-72-2021) for financial support. Computational resources for the simulations were provided by the DeiC National HPC Center, SDU.

[1] W. P. Levin, H. Kooy, J. S. Loeffler, and T. F. DeLaney, *Br. J. Cancer* **93**, 849 (2005).

[2] U. Amaldi and G. Kraft, *Rep. Prog. Phys.* **68**, 1861 (2005).

- [3] E. Surdutovich and A. V. Solov'yov, *Eur. Phys. J. D* **68**, 353 (2014).
- [4] P. Bræmer-Jensen and U. I. Uggerhøj, *Kvant* **2**, 13 (2017).
- [5] W. Bragg, *The London, Edinburgh, and Dublin Philosophical Magazine and Journal of Science* **8**, 726 (1904).
- [6] W. H. Bragg and R. Kleeman, *The London, Edinburgh, and Dublin Philosophical Magazine and Journal of Science* **10**, 318 (1905).
- [7] E. Surdutovich, O. Obolensky, E. Scifoni, I. Pshenichnov, I. Mishustin, A. V. Solov'yov, and W. Greiner, *Eur. Phys. J. D* **51**, 63 (2009).
- [8] E. Surdutovich and A. V. Solov'yov, *J. Phys.: Conf. Ser.* **438**, 012014 (2013).
- [9] A. Verkhovtsev, E. Surdutovich, and A. V. Solov'yov, Predictive assessment of biological damage due to ion beams, in *Nanoscale Insights into Ion-Beam Cancer Therapy*, edited by A. V. Solov'yov (Springer International Publishing, Cham, 2017), pp. 359–377.
- [10] A. Solov'yov, *Nanoscale Insights into Ion-Beam Cancer Therapy* (Springer, New York, 2017).
- [11] A. Verkhovtsev, E. Surdutovich, and A. V. Solov'yov, *Sci. Rep.* **6** (2016).
- [12] W. Kohn, *Rev. Mod. Phys.* **71**, 1253 (1999).
- [13] P. Atkins and R. Friedman, *Molecular Quantum Mechanics*, 4th ed. (Oxford University Press, Oxford, UK, 2005), Vol. 1.
- [14] M. A. L. Marques, N. T. Maitra, F. M. S. Nogueira, E. K. U. Gross, and A. Rubio, *Fundamentals of Time-Dependent Density Functional Theory* (Springer, New York, 2012), Vol. 837.
- [15] E. Runge and E. K. U. Gross, *Phys. Rev. Lett.* **52**, 997 (1984).
- [16] M. J. Frisch, G. W. Trucks, H. B. Schlegel, G. E. Scuseria, M. A. Robb, J. R. Cheeseman, G. Scalmani, V. Barone, B. Mennucci, G. A. Petersson, H. Nakatsuji, M. Caricato, X. Li, H. P. Hratchian, A. F. Izmaylov, J. Bloino, G. Zheng, J. L. Sonnenberg, M. Hada, M. Ehara *et al.*, Gaussian 09 Revision E.01, Gaussian, Inc., Wallingford, CT, 2009.
- [17] T. Yanai, D. P. Tew, and N. C. Handy, *Chem. Phys. Lett.* **393**, 51 (2004).
- [18] G. A. Petersson, A. Bennett, T. G. Tensfeldt, M. A. Al-Laham, W. A. Shirley, and J. Mantzaris, *J. Chem. Phys.* **89**, 2193 (1988).
- [19] M. Marques, A. Castro, G. F. Bertsch, and A. Rubio, *Comput. Phys. Commun.* **151**, 60 (2003).
- [20] A. Castro, M. Oliveira, C. Rozzi, X. Andrade, F. Lorenzen, M. Marques, E. Gross, and A. Rubio, *Phys. Status Solidi B* **243**, 2465 (2006).
- [21] X. Andrade, D. Strubbe, A. Larsen, M. J. T. Oliveira, J. Alberdi-Rodriguez, A. Varas, I. Theophilou, N. Helbig, M. Verstraete, L. Stella, F. Nogueira, A. Aspuru-Guzik, A. Castro, M. A. L. Marques, and A. Rubio, *Phys. Chem. Chem. Phys.* **17**, 31371 (2015).
- [22] J. P. Perdew and A. Zunger, *Phys. Rev. B* **23**, 5048 (1981).
- [23] X. Xu and W. A. Goddard III, *Proc. Natl. Acad. Sci. USA* **101**, 2673 (2004).
- [24] A. Castro and M. A. L. Marques, *Lect. Notes Phys.* **706**, 197 (2006).
- [25] See Supplemental Material at <http://link.aps.org/supplemental/10.1103/PhysRevA.98.012702> for details of the system setup of the C4+ ion collisions with the CYT+GUA pair target. Furthermore, the document lists the descriptions of several animations of the collision process, recorded for varying impact parameter and the collision angle.
- [26] R. L. Snow and J. L. Bills, *J. Chem. Educ.* **52**, 506 (1975).
- [27] E. C. Montenegro and H. Luna, *Braz. J. Phys.* **35**, 927 (2005).